The lightning swept stroke along an aircraft in flight. Part II: numerical simulations of the complete process

Larsson, A; Lalande, P; Bondiou-Clergerie, A

Published in:
Journal of Physics D: Applied Physics

DOI:
10.1088/0022-3727/33/15/318

2000

The lightning swept stroke along an aircraft in flight. Part II: numerical simulations of the complete process

2000 J. Phys. D: Appl. Phys. 33 1876

(http://iopscience.iop.org/0022-3727/33/15/318)

J. Phys. D: Appl. Phys. **33** (2000) 1876–1883. Printed in the UK PII: S0022-3727(00)11284-7

The lightning swept stroke along an aircraft in flight. Part II: numerical simulations of the complete process

Anders Larsson†, Philippe Lalande and Anne Bondiou-Clergerie‡

Office National d'Etudes et de Recherches Aérospatiales,
BP 72–29 Avenue de la Division Leclerc, F-92322 Châtillon CEDEX, France

E-mail: bondiou@onera.fr

Received 2 May 2000

Abstract. During a lightning strike to an aircraft in flight, the lightning channel gets deformed in the airflow and displaced along the aircraft, a so-called *swept stroke*. The deformation and the displacement are caused by the interaction between the aerodynamic flow and the plasma properties of the channel together with the properties of the surface. We give a theoretical analysis and a numerical modelling of the swept-stroke processes. Some numerical simulations of the swept stroke are presented and the results are compared with existing experimental data with satisfying agreement.

1. Introduction

In the first part of this work (Larsson *et al* 2000) we described in a qualitative way what happens when lightning strikes an aircraft in flight and how the lightning channel sweeps along the body of the aircraft. Furthermore, a detailed analysis of the properties of the lightning arc channel was also included. In this paper, the details of the above-mentioned qualitative description are scrutinized and quantified, resulting in a theoretical description of the lightning swept stroke along an aircraft. This description is implemented into a numerical tool and calculations are compared with existing experimental data.

Within the swept-stroke process, the following sub-problems are identified:

(a) the properties of the lightning channel;
(b) the attachment point phenomena;
(c) the reattachment process;
(d) the aerodynamic flow;
(e) the discharge current;

where (a) includes the electrical and thermal properties of the arc plasma; (b) the surface properties and the interaction between the surface and the arc plasma; (c) the properties of electrical breakdown; and (d) the fluid dynamic properties of the aerodynamic flow. (e) is regarded as a boundary condition and is thus required as input data to the simulations. These sub-problems are analysed and discussed in sections 2–6. The main algorithm and three examples of complete swept-stroke simulations are given in section 7. SI units are used in all the equations throughout this paper. When the original references gave formulae in non-standard units, the formulae have been converted into proper ones.

2. Channel properties

The most important parameters of the lightning channel are its internal electric field and its radius. The internal electric field is needed to calculate the voltage distribution along the channel, a voltage distribution that is required for the calculation of possible reattachments (section 4). The channel radius is of importance in the discussion of the influence of the boundary layer (sections 3 and 5). In the first part of this work (Larsson *et al* 2000), the properties of the lightning channel during the continuous current phase of the lightning swept stroke were analysed in detail. This analysis demonstrated that an appropriate definition of the position of the channel is the position of its temperature maximum (Maecker 1971) and that the channel can be considered to be a free-burning arc subjected to increased thermal losses due to a transverse aerodynamic flow (Bublievskii 1978). For a free-burning arc without any transverse aerodynamic flow, the internal electric field is in the range 200–150 V m^{-1} for arc currents of 100 A–1 kA and the channel radius is in the range of 20–60 mm for the currents and the timescale of interest. However, when having a transverse aerodynamic flow, the internal electric field E and the channel radius r are given by

$$E = 1.83 \times 10^3 \left(\frac{v^2}{I}\right)^{1/3} \tag{1}$$

† Postdoctoral researcher at ONERA. Present affiliations: Division of Atomic Physics and Division of Combustion Physics, Lund Institute of Technology, PO Box 118, S-221 00 Lund, Sweden.
‡ Author to whom correspondence should be addressed: Office National d'Etudes et de Recherches Aérospatiales, BP 72–29 Avenue de la Division Leclerc, F-92322 Châtillon, CEDEX France, Fax: +33 1 46 73 41 48.

0022-3727/00/151876+08$30.00

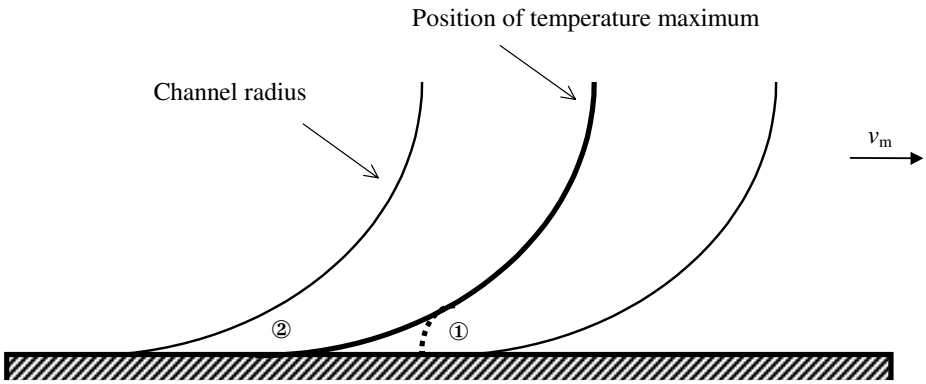

Figure 1. An explanation of the continuous motion of the attachment point of an arc channel where v_m is the aerodynamic flow velocity. The current density is higher in region ① than in region ② since ① forms a shorter electrical path for the current. Thus, more Joule heat is deposited in region ①, resulting in a displacement of the position of the temperature maximum into this region. The bold full curve is the position of the temperature maximum located at the centre of the channel. The broken curve is the displacement of this position downstream due to the non-uniform heating.

and

$$r = 1.50 \times 10^{-4} \left(\frac{I^2}{v} \right)^{1/3} \tag{2}$$

where I is the current and v is the speed of the transverse aerodynamic flow.

3. Attachment point phenomena

The phenomena that occur at the attachment points where the interphase between plasma conduction and metal conduction are located are diverse and complex. Fortunately, for the present study, details of the local interphasial processes are not of interest; only the question of how these processes influence the movement of the attachment point has to be addressed. Most of the surface effects are so localized that they can be neglected. One example of such neglected effects is the random motion that has been observed for both cathodic and anodic spots. Further examples are the voltage drop (of the order of ten volts) and the thickness (of the order of one mean free path of ions or electrons) of the cathodic layer (Raizer 1997).

3.1. Bare metal surfaces

Laboratory experiments (Oh and Schneider 1975, Bizyaev *et al* 1999) show that the discharge channel either sweeps continuously along a bare metal surface or that it dwells shortly (a few milliseconds) at each attachment point. The continuous sweeping can be understood in the following way (figure 1). As mentioned in section 2, the position of the arc channel is defined as the position of the maximum temperature. The aerodynamic flow distribution, in particular the structure of the boundary layer, will deform the channel in the vicinity of the surface. A consequence of this deformation is that the current density at the attachment point will be concentrated downstream of the channel, resulting in an increased heating of this part of the channel. Thus, the position of the maximum temperature will be displaced in the direction of the aerodynamic flow. The thickness of the boundary layer together with the channel radius determine the region of continuous sweeping. If the channel radius is equal to or greater than the boundary layer thickness, the channel can be assumed to follow the background flow above the boundary layer.

If the surface is not perfectly smooth, but contains rivets, joints, etc, there might be preferred attachment points where the attachment point of the channel can dwell. But existing experimental data appear to be contradictory. Oh and Schneider (1975) report that the channel neither dwells at nor is influenced by surface discontinuities or irregularities. On the other hand, Bizyaev *et al* (1999) report the contrary. Because of lack of detailed and unambiguous experimental data, the presence of surface irregularities is not further considered in the modelling presented here. However, future research will address this issue.

3.2. Painted metal surface

A painted surface is a metallic electrode covered with a dielectric layer. To have an attachment point at a painted surface, the paint layer must be punctured. The breakdown voltage of such a layer is typically 1 kV (Dobbing and Hanson 1978). This value is too low to prevent, or even inhibit, the lightning discharge establishing a first attachment point. As in the case of a bare metal surface, the current at the attachment point will be concentrated downstream from the channel. However, the dielectric paint layer inhibits the current further downstream and the current at the attachment point is limited to the area of the hole of the puncture. Thus, the continuous sweeping is prevented by the paint layer and the attachment point dwells at the same spot. Consequently, the channel gets elongated and deformed by the distribution of the aerodynamic flow.

4. Reattachment

Reattachment occurs when the potential drop along the channel together with the channel displacement and deformation due to the aerodynamic flow create a situation where there is a favourable condition for an electrical breakdown between a segment of the channel and the surface

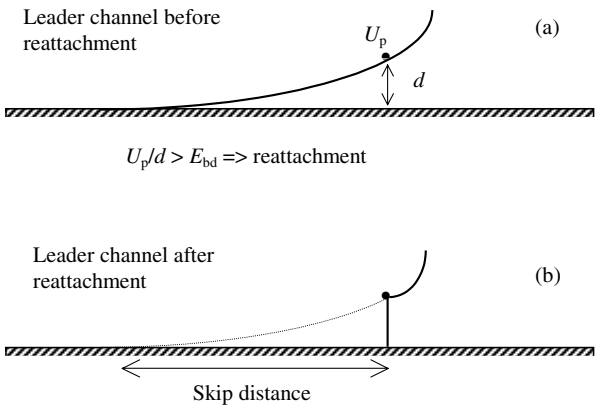

Figure 2. The reattachment process. If the voltage between some segment of the channel and the surface becomes too high, the gap between them breaks down and short-circuits a part of the old channel (broken curve). The attachment point makes a jump (the skip distance).

(figure 2). After the reattachment, the channel has a new attachment point and part of the channel is short-circuited. The distance between two consecutive attachment points is called the 'skip distance'. Figure 2 illustrates a reattachment along a plane surface. For a more complex geometry such as an aircraft, the attachment point may jump far, for instance from the fuselage to the engine. If the metallic surface is painted, the gap between the channel and the surface can be seen as two sub-gaps in series, one air gap and one gap consisting of the dielectric paint layer. The total breakdown voltage U_{bd} can then be expressed as the sum of the breakdown voltages of the sub-gaps

$$U_{bd} = U_{bd,air} + U_{bd,paint}. \tag{3}$$

The technique for calculating the electric field distribution during a lightning strike to an aircraft is highly developed (Castellani 1995). Further, detailed air discharge models also exist (see, for instance, Bazelyan and Raizer (1998)). A combination of an advanced field calculation program with a detailed air discharge model would solve the problem of reattachment to a high degree of accuracy. However, here we have chosen the most simple air breakdown model possible. From the channel internal electric field given by equation (1), the potential of each point along the channel is determined. The potential difference between the channel at each point is divided by the closest distance to the aircraft. If this mean electric field is above a certain critical value, there will be a breakdown between the channel and the surface, that is, a reattachment occurs and a new attachment point is created.

5. Aerodynamic flow

To solve the general problem for the aerodynamic flow distribution around such a complex object as an aircraft in flight, the full nonlinear Navier–Stokes equation must be solved including effects such as boundary layers, wakes, turbulence, supersonic flow, etc. Even if the problem is well-defined, the complete problem is too complex and requires too fine a mesh to be numerically solvable with today's computers. However, within the scope of this paper, the interest is limited to the general behaviour of the aerodynamic flow around the object and appropriate simplifications can be made.

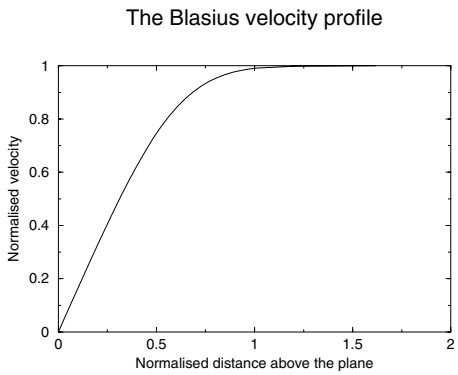

Figure 3. The aerodynamic flow velocity for a flow above a plane surface as a function of the distance above the surface, where the undisturbed flow is directed parallel to the surface (the Blasius velocity profile). The velocity is normalized with the undisturbed aerodynamic flow velocity. The distance above the plane is normalized with the position where the aerodynamic flow velocity is 99% of the undistorted flow velocity (that is, normalized with the thickness of the boundary layer).

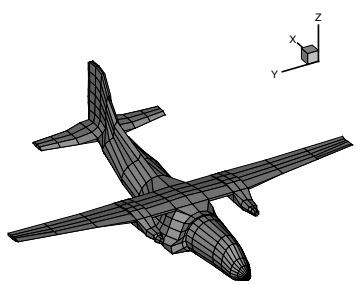

Figure 4. The meshed Transall aircraft. This meshing was used in the calculation of the aerodynamic velocity distribution used in the swept-stroke simulations presented in section 7.3.

For the calculated examples of an aerodynamic flow above a plane surface (sections 7.1 and 7.2), a flow velocity distribution according to the Blasius profile has been used (Schlichting 1968). This velocity profile is shown in figure 3.

The aerodynamic flow around such a complex object like an aircraft in flight (section 7.3) must be explicitly calculated. To simplify these calculations, the aerodynamic flow is assumed to be steady, incompressible and inviscid. These are valid assumptions outside of the boundary layer. The boundary layer is normally defined as the region close to a surface where the aerodynamic flow velocity is less than 99% of the undistorted aerodynamic flow velocity (Tritton 1988). The thickness of the boundary layer around an aircraft in flight is typically 10–20 mm or less. This thickness is of the same order of magnitude as the channel radius (section 3). To simplify the situation we assume that the thickness of the boundary layer is smaller that the radius of the channel which allows us to make the assumption of continuous sweeping throughout the whole boundary layer. A detailed model of the boundary layer will be the subject of future research. If assuming the three conditions mentioned above, one is

Table 1. The characteristics of the continuous current phase of a lightning strike to an aircraft as presented by Lalande *et al* (1999). The data is achieved from in-flight measurements.

	Average	Standard deviation	Min	Max
Duration (ms)	188	±156	34	510
Mean magnitude (A)	330	±285	100	1200
Max magnitude (A)	910	±1023	150	5100

allowed to introduce a quantity ϕ (the velocity potential) such that $\boldsymbol{u} = \nabla\phi$ where $\boldsymbol{u}$ is the velocity field (Lamb 1945). The velocity potential obeys the Laplace equation $\nabla^2\phi = 0$. Techniques for solving the Laplace equation are highly developed as a result of its importance in a variety of other physical contexts. We have chosen to solve it with an integral method, utilizing Green's integral representation (Gasser 1994). One reason for this choice is that with such a method, the heavy calculation is to determine the sources and once they are established, the flow velocity can be readily calculated wherever needed. This is a very efficient approach for our problem since we do not know in advance where the lightning channel will be swept and thus do not know *a priori* at which points the flow velocity is required. The aircraft is divided into rectangular elements (figure 4). Initially, the source terms for each element are calculated and stored. These source terms are then used in the swept-stroke simulation for calculation of the flow velocity for each point along the lightning channel. Gasser (1994) gives the equations used for these calculations.

6. The discharge current

For the lightning swept stroke, the thundercloud can be seen as a very stiff current source with a current given by measurements of the lightning current. The distortion of the lightning channel that the aircraft introduces during the swept stroke is negligible in comparison with the total length of the channel. Thus, the lightning current can be imposed as a boundary condition. Table 1 contains a compilation of the characteristics of the lightning current during its continuous current phase. These characteristics were extracted from in-flight measurements (Lalande *et al* 1999). However, for swept-stoke experiments performed in the laboratory, a high-current arc generator provides the discharge current. Such generators are often far from ideal, thus giving a current that is dependent on the discharge development. To correctly model this situation, the model of the discharge channel must be coupled to an equivalent-circuit model of the current generator. If the current from the generator is practically identical for subsequent discharges, a simplification would be to use the measured current as an imposed boundary condition instead of including an equivalent circuit, as done for the lightning swept stroke. If imposing a measured current, one must, however, be very careful when interpreting the calculated results for conditions other than those where the current waveform has been verified.

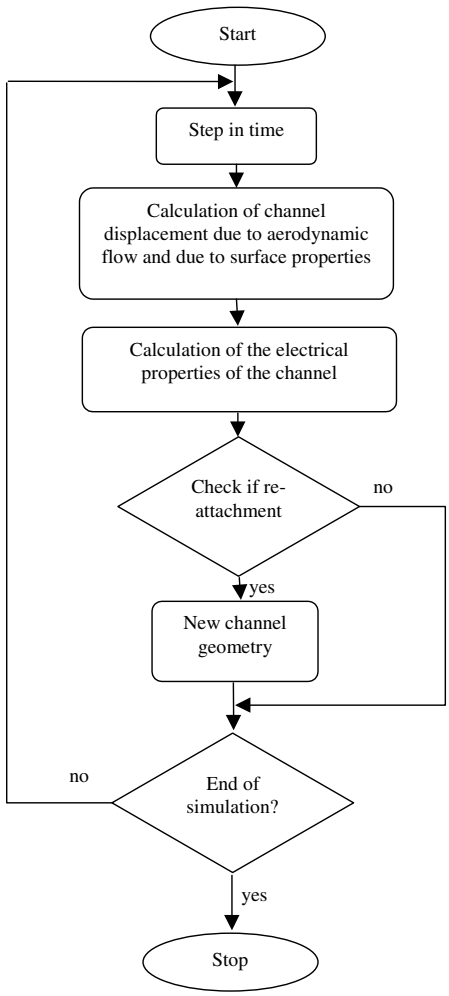

Figure 5. The general algorithm for a swept stoke calculation.

7. Swept-stroke simulations

In this section, three examples of numerical simulations of the swept stroke are presented. The first example is an illustrative one in order to show typical features of a swept stroke. The second is a simulation of a swept-stroke experiment performed by Dobbing and Hanson (1978). The last example is a simulation of the swept stroke along an aircraft in flight, illustrating how the attachment point moves along a complex three-dimensional object. All calculations follow the general algorithm as outlined in figure 5: At each time step, the channel is displaced by the aerodynamic flow and the voltage distribution along the channel is calculated. To determine if reattachment occurs, the distance between the object and each segment of the channel is calculated. The potential at each segment is divided by the distance to the surface and compared with the criterion for breakdown.

7.1. Illustrative example

To illustrate the features of a swept stroke on both unpainted and painted metal surfaces, the following conditions were imposed. The surface was planar and consisted of firstly a bare metal section (0–1 m), then a painted metal section

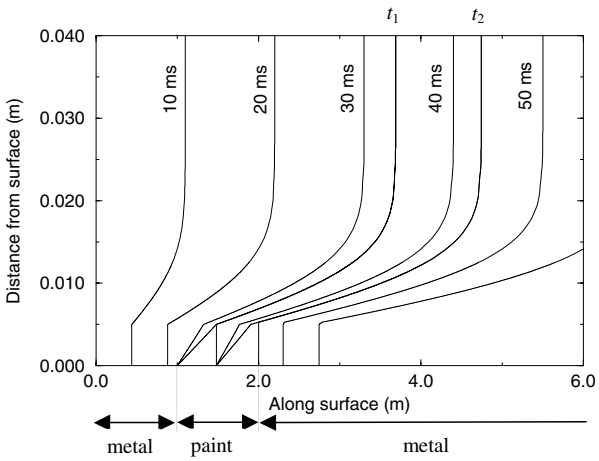

Figure 6. An illustrative swept-stroke simulation. The figure shows snapshots of the position of the temperature maximum of the channel at different times. The lighter curves represent the position of the channel just before and just after a reattachment. At the bottom of the figure, the surface conditions (bare metal or painted) are indicated. The motion of the channel is discussed in detail in the text. Note the different scales on the axes.

(1–2 m) and finally a bare metal section (2 m and onward). The surface was displaced with a speed of 110 m s^{-1} intercepting a steady-state arc with a radius of 5 mm and a current of 500 A. The thickness of the boundary layer was 20 mm.

For the calculations, the following considerations were made:

- The position of the channel is identical to the position of the temperature maximum (section 2).
- Even if it is the surface that was moving, the frame of reference in the calculation is the surface, a surface subjected to an aerodynamic flow.
- Since the surface was a plane, the aerodynamic flow velocity distribution according to the Blasius profile was used for the calculation of the displacement and the deformation of the channel (section 5).
- The region of continuous sweeping over a bare metal surface is equal to the radius of the channel. That is, the velocity of the attachment point is the same as the flow velocity at a height equal to one channel radius.
- No continuous sweeping is present along the painted section of the surface. The attachment point dwells until a reattachment punctures the painted layer downstream.
- The channel is assumed to be subjected to a transverse aerodynamic flow velocity of $(v - v_b)$ where v is the velocity of the surface and v_b is the velocity according to the Blasius profile. This velocity is used in expression (1) to calculate the internal electric field in the channel.

Figure 6 shows the position of the channel at different times. The bold curves represent the position at equidistant time intervals and the thin ones the position just before and just after a reattachment. Note the different scales on the x- and y-axes. At $t = 10$ ms and $t = 20$ ms, the channel appears as a vertical line between $y = 0$ and $y = 5$ mm, representing the continuous sweeping along a bare metal surface for a channel with a radius of 5 mm. At $t = 30$ ms, the channel has arrived at the painted surface and the attachment point dwells at the border between the bare metal surface and the painted surface. At $t = t_1 = 33.5$ ms, the painted layer is punctured and a reattachment occurs at $x_1 = 1.48$ m. The dwell time at the border is 3.5 ms and the skip distance 0.48 m. At $t = 40$ ms, the attachment point still dwells at the punctured hole but at $t = t_2 = 43.1$ ms, the channel makes a reattachment to the second border between the painted surface and the bare metal surface ($x_2 = 2$ m). The dwell time at the punctured hole was 9.6 ms and the skip distance was 0.62 m. At $t = 50$ ms and onwards, the channel continuously sweeps along the bare metal surface. Since the channel radius is smaller than the thickness of the boundary layer, the channel is strongly deformed even during the continuous sweeping phase (for instance, for $t \geqslant 50$ ms), and a reattachment is possible. However, such a reattachment does not occur in the example shown in figure 6.

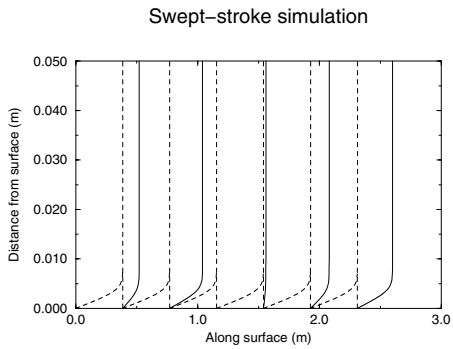

Figure 7. A calculation of a swept stroke along a painted surface with an aerodynamic flow velocity of 52 m s^{-1} and an arc current of 600 A where the channel radius is greater than the thickness of the boundary layer. The full curves are snapshots of the position of the arc channel at regular time intervals (time interval between snapshots: 10 ms). The broken curves show the arc channel just before and just after a reattachment. Note the different scales on the axes.

7.2. Rocket-sled experiment

As mentioned in the first part of this work (Larsson *et al* 2000), Dobbing and Hanson (1978) performed a swept-stroke experiment where they let a surface intercept with a stationary and free-burning arc channel. The surface was a painted wing dummy mounted on a rocket sled running on a railway track. They measured a mean voltage gradient in the arc of $E_{arc} = 1.34 \pm 0.44$ kV m^{-1} for continuous arc currents in the range of 300–600 A and for a rocket sled speed of 52 m s^{-1}. They observed that the arc channel was in contact with the surface along the whole part of the channel that was deformed by the boundary layer, which implies that the thickness of the boundary layer was smaller than the channel radius. The simulation of the rocket-sled experiment was performed in a similar manner as the illustrative example above. However, since the wing dummy was painted, no continuous sweeping was present. Figure 7 shows a swept-stroke calculation with an aerodynamic flow velocity of 52 m s^{-1} and an arc current of 600 A. The thickness of the boundary layer is 5 mm. In the figure, the position of the temperature maximum is shown. The calculation gives a mean voltage gradient of 1.8 kV m^{-1}

Table 2. The influence of aerodynamic flow speed.

Flow speed	Voltage gradient	Skip distance	Dwell time
25 m s^{-1}	1.1 kV m^{-1}	0.62 m	25 ms
52 m s^{-1}	1.8 kV m^{-1}	0.39 m	7.4 ms
75 m s^{-1}	2.3 kV m^{-1}	0.30 m	4.0 ms

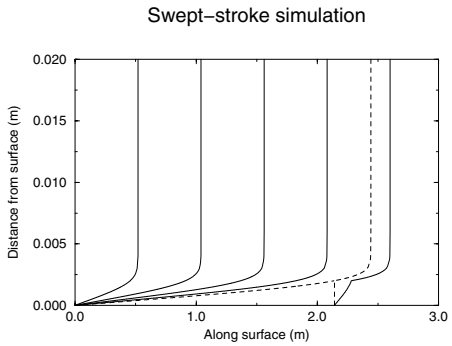

Figure 8. A similar simulation as in figure 7, but with a channel radius that is smaller than the thickness of the boundary layer. The air gap between the channel and the surface increases the breakdown voltage, which results in increased dwell time and increased skip distance.

of the short-circuited part of the arc channel at reattachment (dwell time 7.4 ms, skip distance 0.39 m). This value of the voltage gradient is only slightly higher than the measured one.

If the flow speed is increased, the internal field of the arc channel will increase due to increased thermal losses, leading to an increased average voltage gradient along the short-circuited part of the channel and decreased skip distance and dwell time. Table 2 gives a few calculated examples. These results could not be verified due to lack of experimental data.

If the channel radius is smaller than the thickness of the boundary layer, the geometry of the bent channel leads to the presence of an air gap between the channel and the surface. The air gap significantly increases the breakdown voltage and longer skip distances and longer dwell times will result. These phenomena were observed in the rocket-sled experiments but were not quantified. As an illustrative example, if the channel radius is set to 0.8 mm (thickness of the boundary layer still is 5 mm), a 52 m s^{-1} flow velocity gives an average voltage gradient of 2.0 kV m^{-1}, a skip distance of 2.1 m and a dwell time of 47 ms. Figure 8 shows that the reattachment now occurs within the boundary layer.

7.3. Swept stroke along an aircraft

The final swept-stroke simulations will illustrate how a lightning channel gets attached to different parts of such a complex body as an aircraft. The computational scheme is identical to the one for the swept-stroke simulation presented in sections 7.1 and 7.2 even if the complexity in the aerodynamic flow calculation and in the calculation of the distance between the lightning channel and the aircraft are increased. The aerodynamic flow distribution is calculated as outlined in section 5, using the meshed Transall aircraft shown in figure 4. The calculation of the distance between

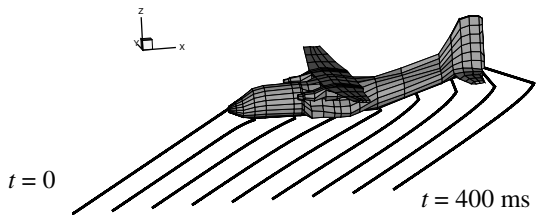

Figure 9. A simulation of the lightning swept stroke to an aircraft in flight. The figure shows snapshots of the position of the lightning channel (the bold curves) at different times (time interval between snapshots: 50 ms). At $t = 0$, the channel has its attachment point at the radome and its direction is given by the vector $(r, \theta, \phi) = (1, 0^\circ, 60^\circ)$ in spherical coordinates. For $t > 0$, it sweeps along the lower part of the fuselage.

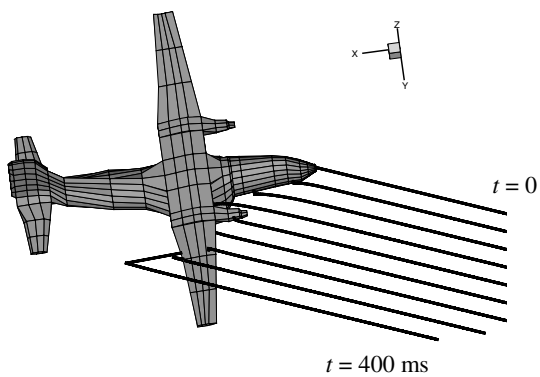

Figure 10. Same as figure 9, but here the channel at $t = 0$ is given by the vector $(r, \theta, \phi) = (1, -30^\circ, 80^\circ)$. For $t > 0$, it sweeps along the fuselage until about $t = 160$ ms when it reattaches to the engine. After the reattachment, the channel sweeps along the engine and eventually along the upper part of the wing.

the lightning channel and the aircraft, and the position on the aircraft where that point is located, is a three-dimensional geometric problem. The calculation procedure is presented in the appendix. Figures 9 and 10 show two examples of how a lightning channel sweeps along the aircraft for an aircraft velocity of 100 m s^{-1}. The first example shows a lightning channel that sweeps underneath the fuselage; a situation similar to the case shown in the video clips presented in figure 3 of the first part of this work (Larsson *et al* 2000). The second one shows how the lightning channel can, when originally being swept along the fuselage, reattach to the engine and further to the wing.

8. Concluding remarks

This paper provides the necessary physical background for a theoretical description of the lightning swept stroke along an aircraft. A few numerical simulations of the swept stroke are presented and the results are compared with experimental data with satisfying agreement. However, due to a lack of detailed and appropriate experimental data, the swept-stroke model could not be thoroughly validated. Hence, to develop an industrial tool for aircraft design, further experimental studies are required. With the knowledge presented in this paper, crucial experiments can be defined. This work has started and experimental campaigns are planned in the near future.

Acknowledgment

The authors thank Nicolas Bettschart for providing the routine that solves their three-dimensional aerodynamic flow problem.

Appendix. Calculation of the channel–surface distance

This appendix describes the algorithm used for the determination of the distance between the lightning channel and the aircraft, and where on the aircraft body it is located. Or in other words, given a point outside a meshed object in three dimensions, what is the (shortest) distance between the point and the object and what are the coordinates on the object giving this distance. The mesh elements are assumed to be triangular.

A.1. The algorithm

To find the distance between the point P and the object, the following algorithm is used

- For each edge

```
Find the point Me on edge's (extended) line which
   is closest to P (section A2)
If Me is located on the edge (section A3)
   store this point
else
   choose the end point of the edge which is closest to P
```

- For each element

```
Find the point Ms on element's (extended) surface
   which is closest to P (section A4)
If Ms is located on the element (section A5)
   store this point
else
   do nothing! (closest point on edge)
```

- Select among the points M_e and M_s that point which gives the shortest distance between P and the object

A.2. Point–line distance

A line through the points $(x_1\ y_1\ z_1)$ and $(x_2\ y_2\ z_2)$ can be given by the parametric vector (Weisstein 1998)

$$\begin{pmatrix} x \\ y \\ z \end{pmatrix} = \begin{pmatrix} x_1 + at \\ y_1 + bt \\ z_1 + ct \end{pmatrix} \qquad \text{with} \quad \begin{pmatrix} a \\ b \\ c \end{pmatrix} = \begin{pmatrix} x_2 - x_1 \\ y_2 - y_1 \\ z_2 - z_1 \end{pmatrix}. \tag{A1}$$

The distance between a point $P = (x_p\ y_p\ z_p)$ outside of the line and an arbitrary point on the line is given by

$$r^2 = (x_p - x_1 - at)^2 + (y_p - y_1 - bt)^2 + (z_p - z_1 - ct)^2. \tag{A2}$$

Let $M = (x_m\ y_m\ z_m)$ be the point on the line that is closest to (or minimize the distance to) the point P. M is then given by

$$\frac{\mathrm{d}}{\mathrm{d}t} r^2 = 0 \Rightarrow t_m = \frac{a(x_p - x_1) + b(y_p - y_1) + c(z_p - z_1)}{a^2 + b^2 + c^2}. \tag{A3}$$

Thus, (A3) in (A2) gives the shortest distance between the point and the line.

A.3. Does the point lie on the edge?

If M is located on the edge, then M is the point on the edge that is closest to P, otherwise the closest point is located on one of the edge's end points. Let the edge's end points be $(x_1\ y_1\ z_1)$ and $(x_2\ y_2\ z_2)$. The point $M = (x_m\ y_m\ z_m)$ on the line lies on the edge if

$$\begin{aligned} &\min(x_1, x_2) \leqslant x_m \leqslant \max(x_1, x_2) && \text{if } a \neq 0 \\ &\min(y_1, y_2) \leqslant y_m \leqslant \max(y_1, y_2) && \text{if } b \neq 0 \\ &\min(z_1, z_2) \leqslant z_m \leqslant \max(z_1, z_2) && \text{if } c \neq 0. \end{aligned}$$

Since the edge is a straight line, it is only necessary to check if one of these three conditions is fulfilled.

A.4. Point–surface distance

Let M be the point on the surface $ax + by + cz + d = 0$ that is closest to point P outside the surface. It follows that the vector $\boldsymbol{MP}$ is normal to the surface and thus is parallel (or antiparallel) to the normal vector $\boldsymbol{N}$ of the surface. If normalizing with the vectors' lengths one gets the following identity

$$\frac{\boldsymbol{MP}}{|\boldsymbol{MP}|} = \operatorname{sign}(\boldsymbol{MP} \cdot \boldsymbol{N}) \frac{\boldsymbol{N}}{|\boldsymbol{N}|} \tag{A4}$$

since

$$\operatorname{sign}(\boldsymbol{MP} \cdot \boldsymbol{N}) \begin{cases} = 1 \rightarrow \textit{parallel} \\ = -1 \rightarrow \textit{antiparallel}. \end{cases}$$

Let $P = (x_p\ y_p\ z_p)^{\mathrm{T}}$. The (closest) distance d between the surface and P is then given by (Weisstein 1998)

$$d = \frac{|ax_p + by_p + cz_p + d|}{(a^2 + b^2 + c^2)^{1/2}} \tag{A5}$$

but $d = |\boldsymbol{MP}|$. With $M = (x_m\ y_m\ z_m)^{\mathrm{T}}$, $\boldsymbol{MP} = (x_p - x_m, y_p - y_m, z_p - z_m)^{\mathrm{T}}$ and $\boldsymbol{N} = (a, b, c)^{\mathrm{T}}$ one gets

$$\begin{aligned} &\frac{1}{|ax_p + by_p + cz_p + d|/(a^2 + b^2 + c^2)^{1/2}} \begin{pmatrix} x_p - x_m \\ y_p - y_m \\ z_p - z_m \end{pmatrix} \\ &= \operatorname{sign}(\boldsymbol{MP} \cdot \boldsymbol{N}) \frac{1}{(a^2 + b^2 + c^2)^{1/2}} \begin{pmatrix} a \\ b \\ c \end{pmatrix} \Rightarrow \begin{pmatrix} x_m \\ y_m \\ z_m \end{pmatrix} \\ &= -\operatorname{sign}(\boldsymbol{MP} \cdot \boldsymbol{N}) \frac{|ax_p + by_p + cz_p + d|}{a^2 + b^2 + c^2} \begin{pmatrix} a \\ b \\ c \end{pmatrix}. \end{aligned} \tag{A6}$$

The term sign $(\boldsymbol{MP} \cdot \boldsymbol{N})$ on the right-hand side of (A6) makes the problem implicit. This is solved by calculating the distance between the point and the surface for both choices of sign. The correct point is then the one with the shortest distance to the surface (a distance which should be zero).

A.5. Does the point lie on the surface?

Let $M = (x_m\ y_m\ z_m)^{\mathrm{T}}$ be the projection of point $P = (x_p\ y_p\ z_p)^{\mathrm{T}}$ on the surface $ax + by + cz + d = 0$. A triangular element on the surface is given by its three nodes $n_i = (x_i\ y_i\ z_i)^{\mathrm{T}}$, $i = 1, 2, 3$. Further, let e_i be the lengths

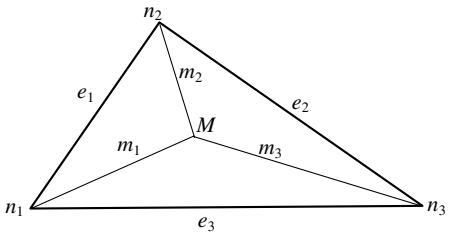

Figure A1. The element and its sub-triangles. The point M can lie either outside or inside of the element. Here is a case where M is located inside the element.

of the sides of the triangular element and m_i the length from each node to the projection M. See figure A1. The projection M lies within the element if the area of the element is equal to the sum of the areas of the sub-triangles. The sub-triangles are the three triangles that can be formed by the projection M together with the nodes n_i of the element.

The area A of the element is given by (Heron's formula)

$$A = \sqrt{s(s-e_1)(s-e_2)(s-e_3)} \qquad s = \tfrac{1}{2}(e_1+e_2+e_3).$$

The areas of the sub-triangles are given by

$$A_1 = \sqrt{s_1(s_1-e_1)(s_1-m_1)(s_1-m_2)}$$
$$s_1 = \tfrac{1}{2}(e_1+m_1+m_2)$$
$$A_2 = \sqrt{s_2(s_2-e_2)(s_2-m_2)(s_2-m_3)}$$
$$s_2 = \tfrac{1}{2}(e_2+m_2+m_3)$$
$$A_3 = \sqrt{s_3(s_3-e_3)(s_3-m_1)(s_3-m_3)}$$
$$s_3 = \tfrac{1}{2}(e_3+m_1+m_3).$$

If $A = A_1 + A_2 + A_3$ then the projection M lies within the element. (If the area A is less than the sum of the areas of the sub-triangles, then the projection lies outside of the element.)

References

Bazelyan E M and Raizer Yo P 1998 *Spark Discharge* (Boca Raton, FL: CRC Press)

Bizyaev A *et al* 1999 Investigation of the sweeping of lightning in wind blown arc experiments *Int. Conf. on Lightning and Static Electricity (Toulouse, France)*

Bublievskii A F 1978 An approximate model of an electric arc in transverse mutually perpendicular aerodynamic and magnetic fields *J. Eng. Phys.* **35** 1424

Castellani A 1995 Calcul du champ électrique par la méthode des charges equivalentes pour la simulation d'une décharge bi-leader *Thèse de doctorat* Université d'Orsay, Paris

Dobbing J A and Hanson A W 1978 A swept stroke experiment with a rocket sled *Int. Symp. on Electromagnetic Compatibility (Atlanta, USA)*

Gasser D 1994 Etude expérimentale et théorique des phenomènes aerodynamiques de l'interaction rotor-fuselage sur l'hélicoptère en vol d'avancement *Thèse de doctorat* Ecole Nationale Supérieure d'Arts et Métiers, Paris

Lalande P, Bondiou-Clergerie A and Laroche P 1999 Analysis of available in-flight measurements of lightning strikes to aircraft *Int. Conf. on Lightning and Static Electricity (Toulouse, France)*

Lamb H 1945 *Hydrodynamics 6/E* (New York: Dover)

Larsson A, Lalande P, Bondiou-Clergerie A and Delannoy A 2000 The lightning swept stroke along an aircraft in flight. Part I: thermodynamic and electric properties of lightning arc channels *J. Phys. D: Appl. Phys.* **33** 1866–75

Maecker H 1971 Principles of arc motion and displacement *Proc. IEEE* **59** 439

Oh L L and Schneider S D 1975 Lightning strike performance of thin metal skin *Conf. on Lightning and Static Electricity (Culham, UK)*

Raizer Yu P 1997 *Gas Discharge Physics* (Berlin: Springer)

Schlichting H 1968 *Boundary-Layer Theory* 6th edn (New York: McGraw-Hill)

Tritton D J 1988 *Physical Fluid Dynamics* 2nd edn (Oxford: Oxford University Press)

Weisstein E W 1998 *CRC Concise Encyclopedia of Mathematics* (Boca Raton, FL: CRC Press)
webpage <http://www.astro.virginia.edu/ eww6n/math>